

Backpropagation-free Training of Deep Physical Neural Networks

Ali MOMENI,¹ Babak RAHMANI,² Matthieu MALLÉJAC,¹ Philipp DEL HOUGNE,³ and Romain FLEURY^{1,*}

¹*Laboratory of Wave Engineering, École Polytechnique Fédérale de Lausanne, Switzerland.*

²*Microsoft Research, 198 Cambridge Science Park, CB4 0AB Cambridge, UK.*

³*Univ Rennes, CNRS, IETR - UMR 6164, F-35000, Rennes, France*

(Dated: April 24, 2023)

Recent years have witnessed the outstanding success of deep learning in various fields such as vision and natural language processing. This success is largely indebted to the massive size of deep learning models that is expected to increase unceasingly. This growth of the deep learning models is accompanied by issues related to their considerable energy consumption, both during the training and inference phases, as well as their scalability. Although a number of work based on unconventional physical systems, such as wave-based frameworks, have been proposed which addresses the issue of energy efficiency in the inference phase, efficient training of deep learning models has remained unaddressed. So far, training of digital deep learning models mainly relies on backpropagation, which is not suitable for physical implementation as it requires perfect knowledge of the computation performed in the so-called forward pass of the neural network. Here, we tackle this issue by proposing a simple deep neural network architecture augmented by a biologically plausible learning algorithm, referred to as "model-free forward-forward training". The proposed architecture enables training deep physical neural networks consisting of layers of physical nonlinear systems, without requiring detailed knowledge of the nonlinear physical layers' properties. We show that our method outperforms state-of-the-art hardware-aware training methods by improving training speed, decreasing digital computations, and reducing power consumption in physical systems, particularly optics. We demonstrate the robustness and adaptability of the proposed method, even in systems exposed to dynamic or unpredictable external perturbations. To showcase the universality of our approach, we train diverse wave-based physical neural networks that vary in the underlying wave phenomenon and the type of non-linearity they use, to perform vowel and image classification tasks experimentally. This work paves the way for the ambitious goals of hybrid training massive physical neural networks, which can offer high-speed and lower energy consumption not only for inference but also during the training phase.

I. INTRODUCTION

Deep learning has emerged as a breakthrough technology with outstanding success in various fields such as vision, natural language processing (NLP), and speech recognition[1, 2]. Although these algorithms attempt to mimic the functioning of the human brain, they are essentially executed on a software level using traditional von Neumann computing hardware. Nevertheless, artificial neural networks (ANNs) based on digital computing are currently experiencing challenges concerning energy consumption and processing speed [3]. An example of the considerable energy usage involved in training language models can be seen in the case of GPT-3, which has 175 billion parameters and required 1.3 GWh of electricity during training [4]. As a result, researchers are increasingly exploring the implementation of ANNs on alternative physical platforms, including but not limited to optics [5–9], spintronic [10, 11], nanoelectronic devices [12–14], and photonic hardware [5, 15], as well as acoustic systems [16, 17]. Currently, two primary methods are mainly used. The first involves designing hardware that implements trained mathematical transformations through strict operation-by-operation mathematical isomorphism, which is mainly aimed at the inference phase of deep learning [18–21]. The second category, known as deep Physical Neural Networks (PNNs), involves training the physical transformations of the hardware directly to execute the desired computations. PNNs offer the potential to create more scalable, energy-efficient, and faster neural network hardware by leveraging physical transformations and challenging the conventional software–hardware division [22, 23].

Increasing the depth of physical networks (deep PNNs) holds great potential for enhancing performance as it leads to an exponential expansion in network expression capabilities [24]. Their training has predominantly relied on a method called backpropagation (BP), which has been highly successful in training software-based ANNs [25]. Yet, there are several reasons why BP is not a suitable choice for PNNs, one of which is the complexity and lack of scalability in the physical implementations of BP operations [26, 27]. Most proposals for PNNs implement BP calculations on an external computer using a digital twin of the physical system, commonly referred to as in-silico training. This usually

* roman.fleury@epfl.ch

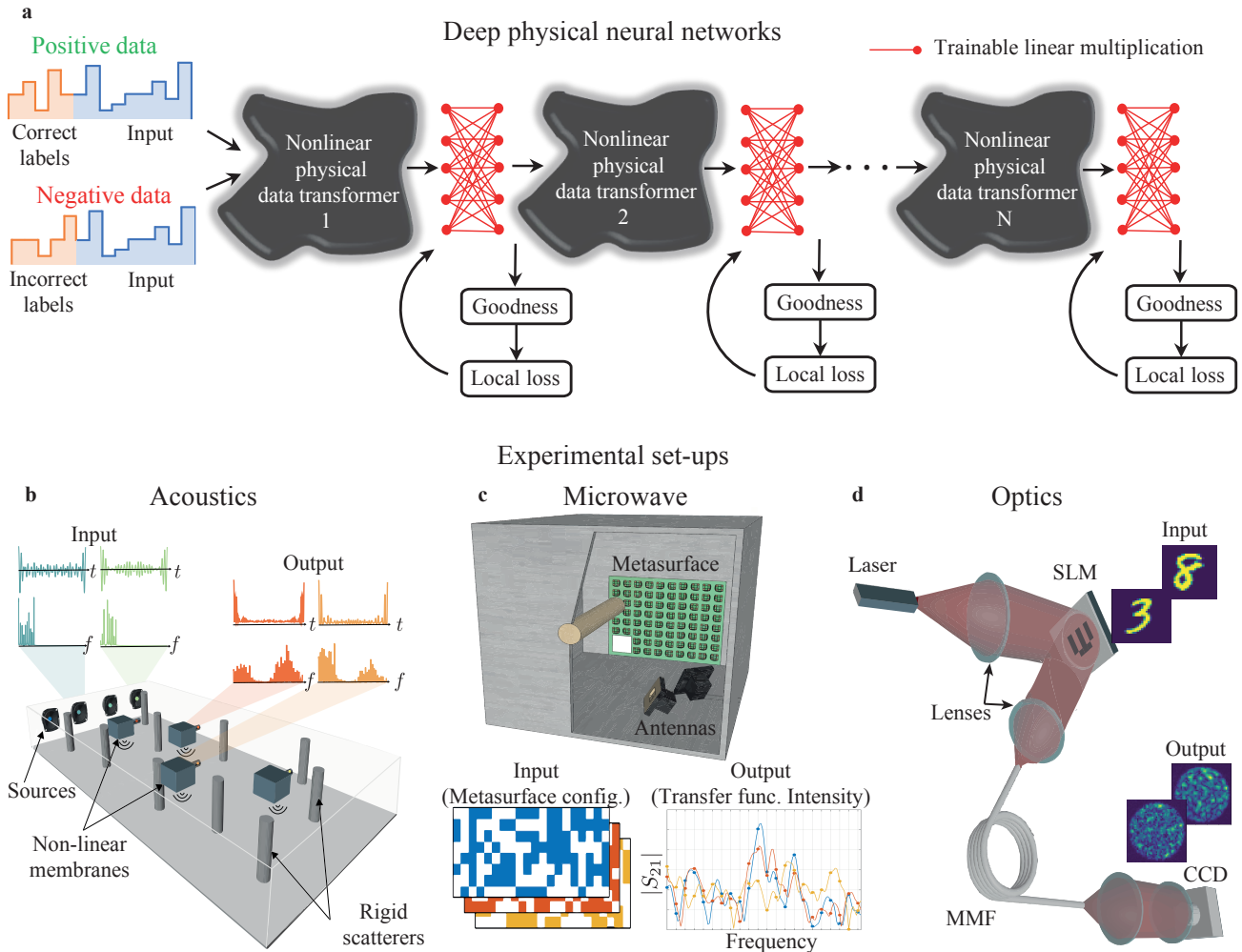


FIG. 1. Deep physical neural networks. **a**, A simple and physics-compatible deep neural network that employs a sequence of nonlinear physical data transformers augmented by trainable matrix multiplications, trained by the model-free forward-forward (MF-FF) technique. At each layer, the nonlinear physical data transformer executes nonlinear mapping between the input and output space, and the MF-FF trains the trainable linear multiplications to determine the optimal decision boundary for positive and negative data. We consider three physical systems that vary in terms of the underlying wave phenomenon and the type of non-linearity. **b**, In acoustics, input data is encoded into the intensity of sound waves at different frequencies injected on the left side of the cavity. Sound waves propagate through a chaotic cavity that comprises multiple rigid cylindrical diffusers and nonlinear membranes. The transformed waveforms are received by multiple microphones. **c**, In the chaotic microwave cavity, input data is encoded into the programmable metasurface configuration inside the metallic disordered cavity. The outputs are obtained from the waves' spectra (transfer function). **d**, In optical setup, input data is encoded onto the SLM, and after passing through the MMF, the resulting optical intensity is measured on the CCD camera.

comes at the cost of speed and an increase in energy consumption during training. Additionally, the model might not accurately represent the real physical system which can lead to a potential simulation–reality gap and unfaithful inference time prediction. [6–8, 10, 13, 14, 20, 28, 29]. Recent work has made some progress towards addressing these issues. The physics-aware training method based on BP (PA-BP) [22] is the current state-of-the-art training framework that circumvents some problems of the in-silico methods. However, the Achilles heel of PA-BP is that it still requires a differentiable digital model for the backward pass. This imposes some limitations on the use cases of the PA-BP, such as the slow training speed, and the high power consumption due to the digital backward pass and the need for extra memory accommodating the backward model of the PNN on a digital computer. Furthermore, as becomes evident later, in the event that the physical system undergoes strong perturbations, retraining PA-BP trained PNNs representing the physical system can be quite challenging.

Another significant drawback of BP is its reliance on having complete knowledge of the computations carried out during the forward pass to accurately compute derivatives [23, 30–33]. When a black box is inserted in the

forward pass, backpropagation becomes impossible. Therefore, researchers are seeking alternative training methods for PNNs. For example, an approach that has been recently explored for training physical networks is the augmented Direct Feedback Alignment (DFA) method [23], which aims to avoid the need for a differentiable digital model. However, this method is only compatible with certain physical networks where the nonlinear and linear layers can be separated. Furthermore, determining the nonlinearity form for PNNs through optimization procedures is still an ongoing challenge.

Here, we propose a simple and physics-compatible PNNs architecture augmented by a biologically plausible learning algorithm, called model-free forward-forward (MF-FF) training. This new route enables direct training of arbitrary PNNs locally without requiring detailed knowledge of the properties of nonlinear physical layers and training a digital model. In this backpropagation-free contrastive learning method, the standard backward pass, typically performed by a digital computer, is replaced with a single forward pass through a physical system. This substitution can significantly improve training speed compared to other hardware-aware training frameworks, reduce digital computations and memory usage, and lower power consumption in the training phase of wave-based PNNs. In this work, we benchmark our learning framework against the state-of-the-art physics-aware training schemes proposed in the literature, i.e., in-silico and backpropagation method. We show the robustness and adaptability of the proposed method compared to its sister schemes, even in systems exposed to unpredictable external perturbations. To showcase the universality of our approach, we perform experimental vowel and image classification using three wave-based systems that differ in terms of the underlying wave phenomenon and the type of non-linearity involved. Our first example consists of a chaotic acoustic cavity implemented with non-linear scatterers. The second example is a chaotic microwave cavity whose transfer function is massively parameterized by a programmable metasurface with structural non-linearity. Our third example is an optical multimodal fiber with readout non-linearity. Our approach results in high-accuracy achieving hierarchical classifiers that make use of the distinct physical transformations of each system and offers a pathway to significantly enhance the energy efficiency and speed of deep learning not only during inference but also during the training phase.

II. RESULTS

A. Model-free forward-forward training

Figure 1a shows a simple and physics-compatible deep PNN including N nonlinear physical data transformers augmented by trainable linear multiplications. Each nonlinear physical data transformer performs a nonlinear mapping between the input and output space “effortlessly”, followed by the use of augmented trainable linear multiplication to classify distinct classes via a local and contrastive training algorithm. The orientation of neuron activities, the output of each layer, is passed to the next layer. The subsequent layer then carries out the same process hierarchically on the output of the previous layer. This architecture shares some similarities with conventional deep Reservoir Computing (deep-RC) systems [34]. However, here all augmented linear multiplications are trained, in contrast to the traditional deep-RC where only the final layer is trained[35, 36]. If nonlinear physical transformations possess some form of memory, the network can be categorized as a trainable deep-RC. Among the various contrastive learning approaches [33], the forward-forward algorithm [30], inspired by Boltzmann machines [37], was recently proposed by Geoffrey Hinton and has undergone further improvement through several proposals in computer science [38, 39]. Here, we implement the model-free version of the forward-forward algorithm, for the aforementioned PNNs-based architecture.

Each nonlinear physical system performs a nonlinear transformation on input data, which can be expressed as $h^{(l)} = f_N^{(l)}(W_p^{(l)}x^{(l)})$, where $x^{(l)}$, $W_p^{(l)}$, and $f_N^{(l)}$ correspond to the physical inputs (e.g., optical intensity, electric voltage, vibration), physical interconnections (e.g., optical, electrical, or mechanical coupling) in the physical system, and physical nonlinearity (e.g., nonlinear optical, magnetic, or mechanical effects) in layer l , respectively. Indeed, $W_p^{(l)}$ and $f_N^{(l)}$ signify mixing operation and non-linear kernel of the l -th physical systems. Afterward, the output of layer l can be expressed as the multiplication of $h^{(l)}$ by the augmented trainable weight matrix $W_t^{(l)}$, $y^{(l)} = W_t^{(l)}h^{(l)}$. Such trainable matrix multiplications can be performed through either digital or physical systems, for instance using Mach-Zehnder Interferometer (MZI) integrated photonics or Spatial Light Modulators (SLMs) in optics[40]. The goal here is to train $W_t^{(l)}$ locally. Instead of a forward and backward pass, here, we use two physical forward passes: a positive and a negative forward pass through the physical systems, each running on different physical inputs. The positive physical pass, $y_{\text{pos}}^{(l)} = W_t^{(l)}f_N^{(l)}(W_p^{(l)}x_{\text{pos}}^{(l)})$, uses positive inputs that include the input dataset and correct labels, while the negative physical pass, $y_{\text{neg}}^{(l)} = W_t^{(l)}f_N^{(l)}(W_p^{(l)}x_{\text{neg}}^{(l)})$, uses negative inputs that include the input dataset and incorrect labels (see Fig. 1a). In each layer, we calculate the so-called “goodness” function, defined as the sum of the

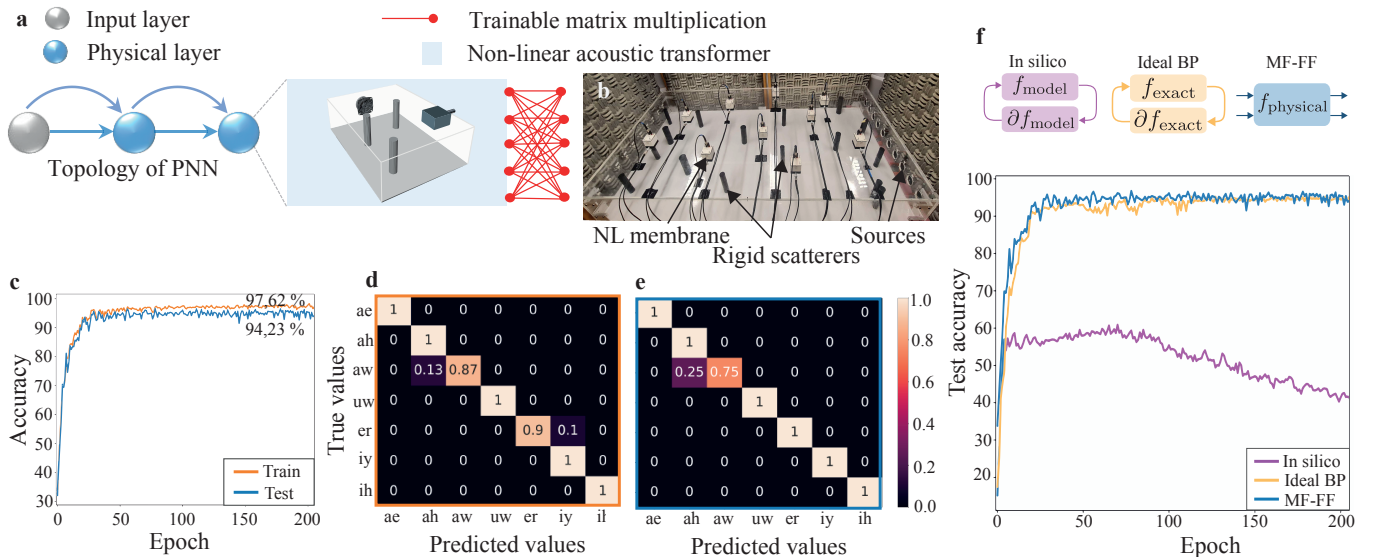


FIG. 2. Acoustic-PNN. **a**, The topology of acoustic-PNN consists of a two-layer PNN with skip connections. Each layer comprises an acoustic-PNN augmented by trainable matrix multiplication. **b**, Photograph of the experimental setup. **c**, The train and test classification accuracy versus training epoch for the vowel recognition task. **d** and **e**, The confusion matrix for the PNN on the train and test set, respectively. **f**, Comparison of test accuracy versus training epoch with in silico, ideal back-propagation, and MF-FF algorithm for the vowel recognition task.

squared activities for the positive and negative physical passes. For instance, in physical systems such as optics, the squared activities correspond to the optical intensity on the CCD camera. Eventually, for each layer 1, $W_t^{(1)}$ is trained by minimizing the following loss function

$$L^{(l)} = \log \left(1 + \exp \left(-\theta \left(\sum_j y_{\text{pos},j}^{(l)} - \sum_j y_{\text{neg},j}^{(l)} \right) \right) \right) \quad (1)$$

where θ is a scale factor. During the inference phase, we input a particular label into the PNNs and accumulate the goodness values for all layers. This process is repeated for each label separately. The label with the highest accumulated goodness value is then selected as the output. The proposed method is also capable of integrating non-differentiable physical systems or components between the layers.

B. Diverse PNNs for vowel and image classification

In Figure 1, we present three deep PNN classifiers for the vowel and MNIST (Modified National Institute of Standards and Technology database) handwritten digit classification task, based on three distinct physical systems. Although there have been proposals that explore wave-based analog computing for linear operations such as multiplication and convolution [41–49], it is important to note that PNNs require nonlinearity to effectively handle a wide range of learning tasks. These tasks include regression and classification, which require nonlinear operations for accurate performance. We consider three wave-based physical systems, each of which features a unique origin of physical nonlinearity and underlying wave phenomenon, highlighting the diversity of physical networks that can be employed. We take advantage of the multiple scattering induced by the disordered environment in these physical systems (chaotic cavities and multimodal fibers) to leverage the mixing process. In addition to provide the required linear mixing, it also helps to intensify the overall nonlinearity [16].

1. Acoustic Chaotic Cavity with Non-Linear Scatterers

In acoustics, an air-filled multimode cavity composed of multiple nonlinear meta-scatterers randomly placed on the cavity top wall and multiple rigid meta-scatterers inside the cavity is employed (see Supplementary Information for more details). The nonlinear meta-scatterers are designed based on an active control strategy. Herein, the

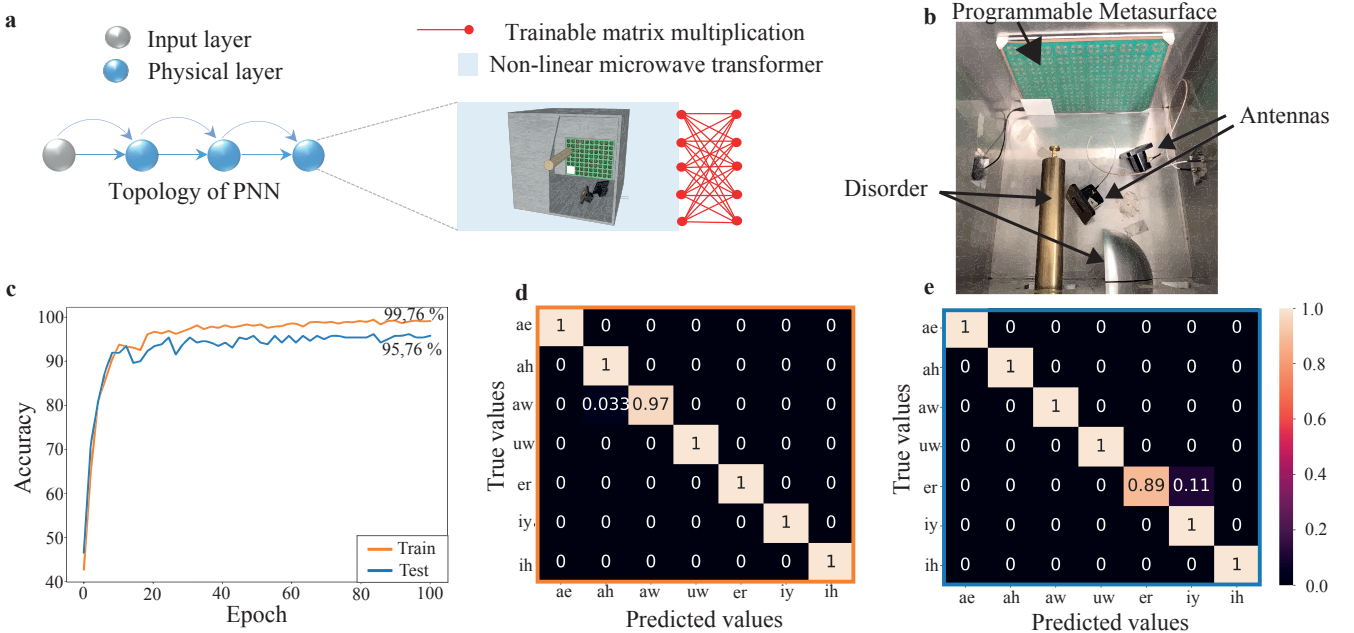


FIG. 3. **Microwave-PNN.** **a**, The topology of microwave-PNN consists of a three-layer PNN with skip connections. Each layer comprises a microwave-PNN augmented by trainable matrix multiplication. **b**, Photograph of the experimental setup. **c**, The train and test classification accuracy versus training epoch for the vowel recognition task. **d** and **e**, The confusion matrix for the PNN on the train and test set, respectively.

positive and negative data are encoded onto the amplitude of each frequency component composing the excitation waveforms, that are then injected into the nonlinear system through loudspeakers positioned on the right side of the cavity. The output of the physical system is measured using microphones below the metascatterers (see Methods and Supplementary Information). We investigate the vowel classification performance of two layers acoustic-PNN (see Fig. 2a). In order to compare the results of MF-FF with ideal BP, and in-silico training, we accurately model the forward pass of acoustic-PPN by a digital neural network (see supplementary information). When the acoustic-PNN is trained using MF-FF, it performs the classification task with 97.62% and 94.23% train and test accuracy, respectively (see Figs. 2c-e). Figure 2f shows the comparison of the classification results obtained for MF-FF, ideal BP, and in-silico training. A schematic visual representation of the aforementioned methods is provided above Fig. 2f (see Supplementary Information for further details).

As evidenced by Fig. 2f, in-silico training performs poorly, reaching only a maximum vowel classification accuracy of $\sim 60\%$. In contrast, MF-FF succeeds in accurately training the acoustic-PNN, performing similarly to the ideal BP algorithm used as a baseline. The key advantage of MF-FF stems from the execution of both forward passes through the physical hardware, rather than simulations.

2. Microwave Massively Parametrized Chaotic Cavity with Structural Non-Linearity

In the microwave regime, we leverage a “structural non-linearity” such that we can implement nonlinear mathematical operations at low power levels with a linear scattering system. Our starting point is an irregularly shaped electrically large metallic enclosure with strong modal overlap. It is coupled via two coax-to-waveguide adapters to two asymptotic scattering channels, and the transfer function between these two channels can be measured using standard equipment such as a vector network analyzer. We then massively parametrize this cavity by covering one of its walls with a programmable metasurface. For each meta-atom and each polarization, we can individually configure the local boundary conditions of the cavity with 1-bit precision (two possible states). Our setup is shown in Fig. 3(b) and very similar to one that was recently used to implement with high fidelity and in situ reprogrammability desired *linear* transfer functions for signal differentiation [50] and routing [51]. In the present work, however, we seek a *non-linear* mapping. Hence, we define the metasurface configuration as the input and the transfer function as the output of our mathematical operation. Indeed, this relation is in general nonlinear due to the mutual coupling between meta-atoms caused by their proximity and, more importantly, the reverberation [52]. While previous work in Ref.[46] sought to limit the reverberation in order to implement a linear transformation with the metasurface configuration as input and

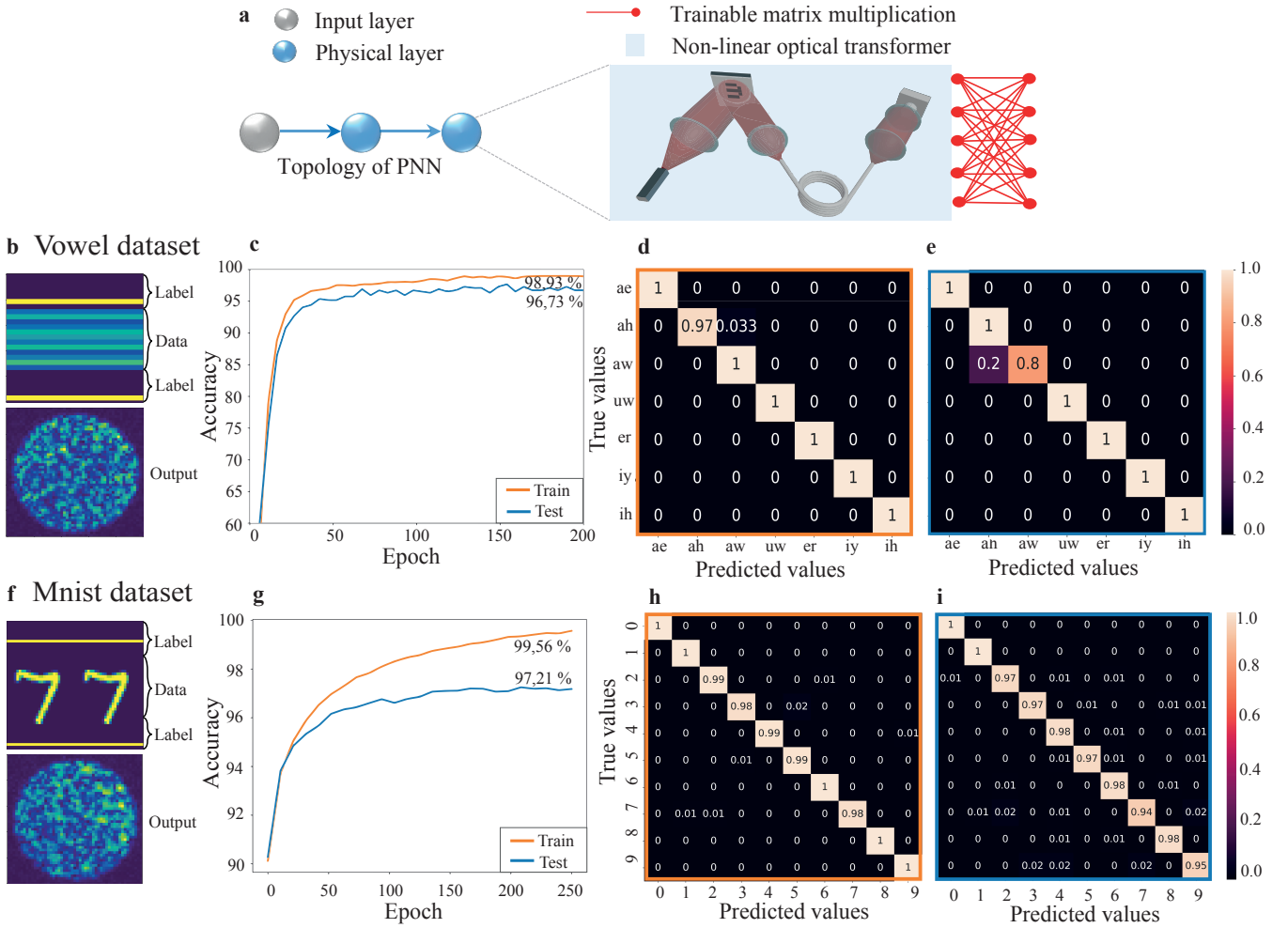


FIG. 4. **Optics-PNN.** **a**, The topology of optics-PNN consists of a two-layer PNN. Each layer comprises an optics-PNN augmented by trainable matrix multiplication. **b** and **f**, An example of input data, including raw data and its label representation on SLM, along with its corresponding output on a CCD camera for vowel and Mnist datasets, respectively. **c** and **g**, The train and test classification accuracy versus training epoch for the vowel recognition and Mnist tasks, respectively. **d** and **e**, The confusion matrix for the PNN on the train and test set for the vowel recognition task, respectively. **h** and **i**, similar results for the Mnist task.

the transfer function as output, here we deliberately seek to maximize the reverberation to boost the nonlinearity. Incidentally, this type of reverberation-induced structural nonlinearity was recently also transposed to the optical domain[53].

We randomly group our programmable metasurface's 152 degrees of freedom into 40 macropixels since our mathematical operation requires 40 inputs. We define our mathematical operation's outputs as the transfer function intensities at twenty decorrelated frequencies within the bandwidth of operation of the programmable metasurface (400 MHz around 5.2 GHz). Note that, in addition to the structural non-linearity, we hence add a readout non-linearity by working with the transfer function's intensity. In order to flexibly evaluate the proposed approach, based on 50000 experimentally measured pairs of a random metasurface configuration and the corresponding transfer function, we learn a digital surrogate forward model of the configuration to transfer function intensity mapping (see Supplementary Information for further details). Then, we construct the three-layer microwave-PNN shown in Fig. 3a and train it according to the MF-FF. The training converges after roughly 20 epochs and the achieved classification accuracy on unseen test data reaches around 96 % (see Figs. 3c-e).

3. Optical Multimode Fiber with Readout Non-Linearity

In the optics part, we use an optical system that comprises an SLM, a scattering medium consisting of a step-index multimode fiber (MMF), and a CMOS camera (see Fig. 1d). In this setup, the positive and negative datasets are encoded onto the SLM, and after passing through the MMF, the resulting optical intensity is measured on the camera. The physical optical system performs a complex spatiotemporal transformation. This transformation involves the propagation of spatially modulated laser pulses through an MMF. The propagation of an ultrashort pulse inside a MMF is a highly complex process that involves spatial and temporal interactions of electromagnetic waves coupled to hundreds of different propagation modes [54, 55]. Although this transformation is linear in the complex domain, the process becomes nonlinear due to the data being encoded onto the phase (SLM) and the subsequent measurement of the intensity squared on the camera. Here, we use a two-layer optics-PNN to perform classification tasks on two different datasets: Vowel and MNIST (see Fig. 4 and Supplementary Information for further details). The optics-PNN achieved an impressive classification performance on both vowel and MNIST datasets. We obtain 98.93% and 96.73% accuracy on the training and test vowel datasets, respectively. Using only two-layer optics-PNN, the model achieves 99.56% and 97.21% accuracy on the training and test Mnist datasets (see corresponding results in Figs. 4c-h). These results demonstrate the ability to transition from an expensive digital processor to a fast, energy-efficient hybrid physical-digital processor, showcasing the potential for optimizing both performance and energy efficiency in machine learning applications.

4. Real-Time Adaptable Learning

We now aim to show the superior robustness of MF-FF in the context of real-time and adaptable learning, where the physical data transformer may undergo changes due to slow dynamics of the physical system during the runtime or external hard perturbations. Let us consider a deep optics-PNN with six layers, as depicted in Fig. 5a, which has already been trained on vowel datasets and is currently in the inference phase. The transformation function of each physical system is $f_o(\theta)$, where θ is the physical input. We perturb the physical systems at a specific time (examples of such perturbations include changes to the state of MMF or the positions of lenses or masks, etc), which results in a change in the transformation function of each physical system from $f_o(\theta)$ to $f_p(\theta)$ (see Fig. 5b). We simply perturb the transmission matrix of the optical setup by adding Gaussian noise with mean μ and standard deviation σ to simulate this situation (see the Supplementary Information for details). As we observe in Fig. 5d, the test accuracy drops as expected after applying the perturbation. The question now is whether the training method can restore the accuracy by retraining the optics-PNN after some epochs. We compare our results with the PA-BP method [22] which uses a digital model for the backward pass and the physical system for the forward pass. As shown in Fig. 5c, PA-BP struggles to restore accuracy with increasing perturbation intensity. For instance, the test accuracy oscillates around 55% for a small perturbation (red dots in Fig. 5c) and worsens further for more intense perturbations. In stark contrast, the proposed MF-FF can easily recover accuracy after a few epochs, regardless of the intensity of the perturbation applied. (see Fig. 5d).

This striking adaptability is owed to the fact that MF-FF executes both forward passes through the physical hardware, rather than digital models. In contrast, the PA-BP method uses a digital model that becomes completely inaccurate after hard-perturbation, necessitating re-training with a new dataset and wasting energy. This study highlights the robustness and adaptability of the proposed model, even in dynamic or unpredictable environments.

III. DISCUSSION

Due to the unprecedented growth in the size of NNs, including models such as GPT 4 with around hundreds of billion parameters, the cost of both the training and inference phases of these networks has increased exponentially. Training of such massive NNs is particularly extremely expensive and time-consuming, with training times taking up to several months. Specialized hardware such as PNNs have the potential to drastically decrease these costs. A few methods have been proposed for training PNNs, but they all face issues such as mismatch between the forward model and the physical system or robustness issues. This is because these methods perform the entire backward pass through a digital computer during training, involving either a digital model in PA-BP or numerical simulations in in-silico training, which can hinder their effectiveness in the training phase. MF-FF enables forward passes through physical systems, resulting in a significant speed-up not only during inference but also in the training phase. Additionally, one prominent advantage of MF-FF training is its robustness to an external perturbation. We observed that the MF-FF training is superior not only to the in-silico training but also to the current state-of-the-art PA-BP method. The performance gap between our method and the PA-BP continues to widen as the depth of the NN increases.

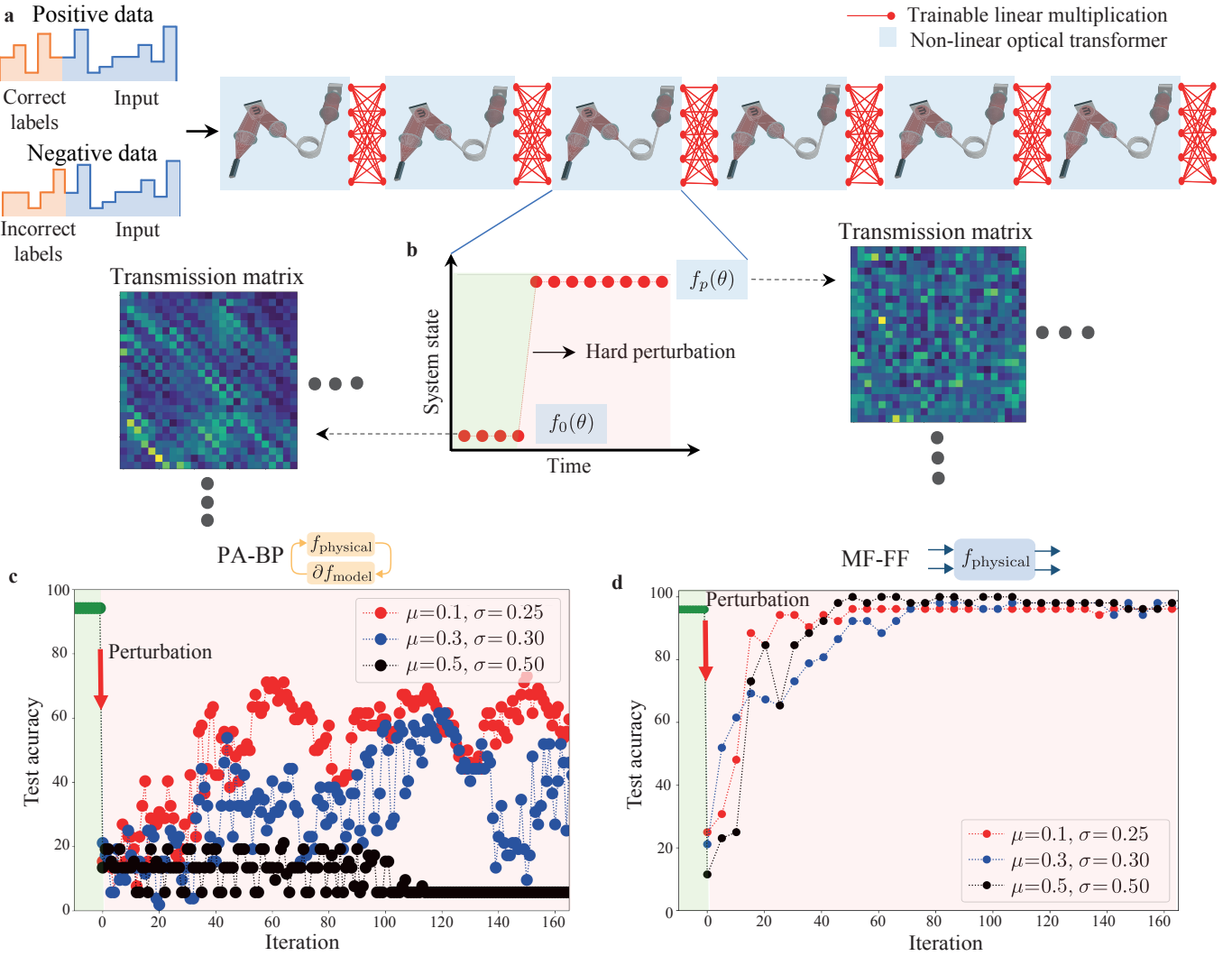


FIG. 5. **Robustness of deep PNNs against unpredictable external perturbations.** **a**, A deep PNN consists of six layers of optics-PNN augmented by trainable matrix multiplication. The deep PNNs trained on vowel datasets and is currently in the inference phase **b**, Applying hard-perturbation by adding Gaussian noise with the mean of μ and standard deviation of σ to the transmission matrix of MMF. **c** and **g**, A comparison between PA-BP [22] and the proposed MF-FF method is presented, with the focus on their ability to recover the classification accuracy after applying perturbation.

This is because, in PA-BP training, the mismatch between the gradients of the non-perturbed and perturbed systems accumulates over the depth of the ANN. Therefore, the more layers a network has, the more sensitive it is to an external perturbation. This is in contrast to the MF-FF trained framework in which each layer of the network is trained separately without using a model.

Despite its many advantages, FF training framework faces some limitations too. In contrast to other PNN training frameworks, MF-FF training requires separate readout of the waves at each layer of the network. To circumvent this issue, we propose a readout mechanism with one wave-to-digital readout hardware shared across the layers. The sequential rather than parallel learning of the FF can particularly easily accommodate this. We further explain this readout mechanism in the supplementary materials.

Although PNNs have the potential to improve deep neural networks' speed and energy consumption to a large extent, a number of challenges still need to be addressed before PNNs can replace their digital counterparts. For example, it is not yet clear how some widely used mathematical operations, such as normalization units, including layer/batch normalization, could be implemented in hardware. Second, how the physical systems could be compactly scaled to billions of parameters. Therefore, we can expect, at least in short term, that PNNs will enable efficient hybrid combinations of in-hardware training/inference rather than a complete replacement for digital processing units.

IV. METHODS

A. Experiments

a. Acoustic system The acoustic system consists of an air-filled cavity 2 m long, 1 m wide and 0.2 m thick supporting 11 propagation modes below 500 Hz. The sealed parallelepiped is instrumented on one side with 10 loudspeakers (Monacor SP6-8SQ) delivering the input waveforms to the system, multiple rigid cylindrical diffusers inside the cavity to increase disorder, and 10 nonlinear resonators (NLRs) randomly positioned on the top layer of the cavity. Each resonator is made up of an electrodynamic loudspeaker (Visator FRWS 5 SC), enclosed in a cavity of volume $V_c = 144 \text{ m}^2$ and an ICP microphone (PCB 130F20, 1/4 inch) placed in front of the diaphragm. From the measured front pressure p_f , a real-time feedback loop assigns a given current $i(t)$ to each NL resonator according to the following control law $i(t) = G_{NL}|p_f(t)|^{\alpha_{NL}}$, where G_{NL} and α_{NL} are two tunable parameters that produce the nonlinearity in the system. The active control is performed on an FPGA-based Speedgoat performance real-time target machine controlled by the xPC target environment of MATLAB/SIMULINK. 4 of the 10 sources are used for training. Each delivers a different linear waveform with a 10 frequencies content in the 350 – 500 Hz range with randomly weighted amplitudes. The output of the system consists of 4 highly non-linear pressure waveforms measured at the output of the active control at 4 different locations. The measurement is performed 10,000 times with different amplitude weighting for each run and each input. The input and output data set therefore consists of two matrices with $40 \times 10,000$ elements.

b. Microwave system Our microwave system is shown in Fig. 3(b) and consists of an irregularly shaped electrically large metallic cavity ($0.385 \text{ m} \times 0.422 \text{ m} \times 0.405 \text{ m}$; 0.0658 m^3) whose scattering properties are massively parametrized through a programmable metasurface. Two waveguide-to-coax adapters (RA13PBZ012-BSMA-F) connect the cavity to two asymptotic scattering channels. The 2-bit programmable programmable metasurface contains 76 meta-atoms that cover 8 % of the cavity surface and efficiently modulate the field inside the cavity within a 400 MHz interval centered on 5.2 GHz. The two bits of control per meta-atom are assigned to the two orthogonal field polarizations. Using a vector network analyzer (Rhode & Schwarz ZVA 67), the transmission spectrum between the two ports is measured. The cavity has a composite quality factor on the order of 370 and around 23 modes overlap at a given frequency [50, 51]. The system's scattering matrix is subunitary due to significant Ohmic losses on the metallic walls. We randomly assign the available 152 1-bit programmable degrees of freedom of our programmable metasurface to 40 groups, coined macro-pixels, since our input vector's dimensions are 1×40 . All meta-atoms within a given macro-pixel are configured identically. We select twenty decorrelated frequencies within the metasurface's operation bandwidth and consider the transfer function intensity at these frequencies as outputs. The relation between inputs and outputs is hence non-linear due to the structural non-linearity [52] and the readout non-linearity. Our use of this microwave setup is distinct from previous works on over-the-air microwave analog computing with programmable metasurfaces in chaotic cavities. While, on the one hand, Ref. [46] also defined a mathematical operation in which the inputs were related to the metasurface configuration and the outputs to the transfer function, it aimed at implementing linear operations and hence sought to minimize the reverberation-induced structural non-linearity whereas we seek to maximize it in the present work. Refs. [50, 51], on the other hand, considered the system's transfer function as the mathematical operation in order to implement desired linear transfer functions for high-fidelity in situ programmable signal differentiation and routing; the inputs in Refs. [50, 51] were hence the incident wavefronts rather than the metasurface configuration.

c. Optical system The data used for the optical experiment are from the published dataset in Rahmani et al. [56]. The optical system therein consists of a spatial light modulator, a scattering medium of a step-index multimode fiber of length 0.75m and core diameter 50 μm with an aperture size 0.22, and a CMOS camera. The entire system is operating at the 532nm and 1 mW power continuous-wavelength light source corresponding to ~ 1050 modes of the fiber for one polarization. Using interferometry measurements [57], a transmission matrix of the optical system is obtained which allows mapping an input 2-dimensional optical field to its complex output field. The columns of the transmission matrix contain the response functions of the system for each of the modes of the fiber, allowing to faithfully calculate the optical responses of the system to arbitrary inputs.

Acknowledgements A.M. and R.F. acknowledge funding from the Swiss National Science Foundation under the Eccellenza grant number 181232. P.d.H. and R.F. acknowledge funding from the ANR-SNF PRCI program (project “MetaLearn”; ANR-22-CE93-0010-01). B.R. acknowledges that all materials pertaining to the optical experiment presented in this manuscript have been sourced from previously published material that is publicly available and was acquired during his tenure at the Laboratory of Applied Photonics Devices at EPFL. This work has no connection to his current employer in any capacity or form.

Contributions A.M. conceived the idea, designed the computational engine, and carried out both the theoretical and numerical simulations as well as a part of the acoustic experiment. B.R. provided the optics data and interpretation of machine learning results. M.M. carried out the acoustic experiment. P.d.H carried out the microwave experiment.

R.F. supervised the project. All authors contributed to the interpretation of the results and the writing of the manuscript.

- [1] Y. LeCun, Y. Bengio, and G. Hinton, *nature* **521**, 436 (2015).
- [2] L. Deng, D. Yu, et al., *Foundations and trends in signal processing* **7**, 197 (2014).
- [3] D. Patterson, J. Gonzalez, Q. Le, C. Liang, L.-M. Munguia, D. Rothchild, D. So, M. Texier, and J. Dean, arXiv preprint arXiv:2104.10350 (2021).
- [4] M. Asghari and A. V. Krishnamoorthy, *Nature photonics* **5**, 268 (2011).
- [5] G. Wetzstein, A. Ozcan, S. Gigan, S. Fan, D. Englund, M. Soljačić, C. Denz, D. A. Miller, and D. Psaltis, *Nature* **588**, 39 (2020).
- [6] X. Lin, Y. Rivenson, N. T. Yardimci, M. Veli, Y. Luo, M. Jarrahi, and A. Ozcan, *Science* **361**, 1004 (2018).
- [7] Z. Wu, M. Zhou, E. Khoram, B. Liu, and Z. Yu, *Photonics Research* **8**, 46 (2020).
- [8] T. W. Hughes, I. A. Williamson, M. Minkov, and S. Fan, *Science advances* **5**, eaay6946 (2019).
- [9] A. Momeni and R. Fleury, *Nature Communications* **13**, 2651 (2022).
- [10] M. Romera, P. Talatchian, S. Tsunegi, F. Abreu Araujo, V. Cros, P. Bortolotti, J. Trastoy, K. Yakushiji, A. Fukushima, H. Kubota, et al., *Nature* **563**, 230 (2018).
- [11] J. Grollier, D. Querlioz, K. Camsari, K. Everschor-Sitte, S. Fukami, and M. D. Stiles, *Nature electronics* **3**, 360 (2020).
- [12] T. Chen, J. van Gelder, B. van de Ven, S. V. Amitonov, B. De Wilde, H.-C. Ruiz Euler, H. Broersma, P. A. Bobbert, F. A. Zwanenburg, and W. G. van der Wiel, *Nature* **577**, 341 (2020).
- [13] H.-C. Ruiz Euler, M. N. Boon, J. T. Wildeboer, B. van de Ven, T. Chen, H. Broersma, P. A. Bobbert, and W. G. van der Wiel, *Nature nanotechnology* **15**, 992 (2020).
- [14] Y. Shen, N. C. Harris, S. Skirlo, M. Prabhu, T. Baehr-Jones, M. Hochberg, X. Sun, S. Zhao, H. Larochelle, D. Englund, et al., *Nature photonics* **11**, 441 (2017).
- [15] L. Appeltant, M. C. Soriano, G. Van der Sande, J. Danckaert, S. Massar, J. Dambre, B. Schrauwen, C. R. Mirasso, and I. Fischer, *Nature communications* **2**, 468 (2011).
- [16] A. Momeni, X. Guo, H. Lissek, and R. Fleury, arXiv preprint arXiv:2304.08380 (2023).
- [17] A. Momeni, X. Guo, H. Lissek, and R. Fleury, in *2022 Sixteenth International Congress on Artificial Materials for Novel Wave Phenomena (Metamaterials)* (IEEE, 2022) pp. X-314.
- [18] G. W. Burr, R. M. Shelby, A. Sebastian, S. Kim, S. Kim, S. Sidler, K. Virwani, M. Ishii, P. Narayanan, A. Fumarola, et al., *Advances in Physics: X* **2**, 89 (2017).
- [19] D. Marković, A. Mizrahi, D. Querlioz, and J. Grollier, *Nature Reviews Physics* **2**, 499 (2020).
- [20] M. Prezioso, F. Merrikh-Bayat, B. D. Hoskins, G. C. Adam, K. K. Likharev, and D. B. Strukov, *Nature* **521**, 61 (2015).
- [21] M. G. Anderson, S.-Y. Ma, T. Wang, L. G. Wright, and P. L. McMahon, arXiv preprint arXiv:2302.10360 (2023).
- [22] L. G. Wright, T. Onodera, M. M. Stein, T. Wang, D. T. Schachter, Z. Hu, and P. L. McMahon, *Nature* **601**, 549 (2022).
- [23] M. Nakajima, K. Inoue, K. Tanaka, Y. Kuniyoshi, T. Hashimoto, and K. Nakajima, *Nature Communications* **13**, 7847 (2022).
- [24] G. F. Montufar, R. Pascanu, K. Cho, and Y. Bengio, *Advances in neural information processing systems* **27** (2014).
- [25] T. P. Lillicrap, A. Santoro, L. Marris, C. J. Akerman, and G. Hinton, *Nature Reviews Neuroscience* **21**, 335 (2020).
- [26] X. Guo, T. D. Barrett, Z. M. Wang, and A. Lvovsky, *Photonics Research* **9**, B71 (2021).
- [27] T. W. Hughes, M. Minkov, Y. Shi, and S. Fan, *Optica* **5**, 864 (2018).
- [28] J. F. Miller, S. L. Harding, and G. Tufte, *Evolutionary Intelligence* **7**, 49 (2014).
- [29] J. Bueno, S. Maktoobi, L. Froehly, I. Fischer, M. Jacquot, L. Larger, and D. Brunner, *Optica* **5**, 756 (2018).
- [30] G. Hinton, arXiv preprint arXiv:2212.13345 (2022).
- [31] H. Zhu, Y. Chen, G. Hu, and S. Yu, *Electronics* **12**, 147 (2022).
- [32] H.-C. Lee and J. Song, arXiv preprint arXiv:2303.08418 (2023).
- [33] R. F. Srinivasan, F. Mignacco, M. Sorbaro, M. Refinetti, A. Cooper, G. Kreiman, and G. Dellaferreira, arXiv preprint arXiv:2302.05440 (2023).
- [34] C. Gallicchio, A. Micheli, and L. Pedrelli, *Neurocomputing* **268**, 87 (2017).
- [35] M. Rafayelyan, J. Dong, Y. Tan, F. Krzakala, and S. Gigan, *Physical Review X* **10**, 041037 (2020).
- [36] J. Dong, M. Rafayelyan, F. Krzakala, and S. Gigan, *IEEE Journal of Selected Topics in Quantum Electronics* **26**, 1 (2019).
- [37] G. E. Hinton, T. J. Sejnowski, et al., *Parallel distributed processing: Explorations in the microstructure of cognition* **1**, 2 (1986).
- [38] G. Zhao, T. Wang, Y. Li, Y. Jin, C. Lang, and H. Ling, arXiv preprint arXiv:2303.09728 (2023).
- [39] A. Ororbia and A. Mali, arXiv preprint arXiv:2301.01452 (2023).
- [40] M. W. Matthès, P. del Hougne, J. De Rosny, G. Leroosey, and S. M. Popoff, *Optica* **6**, 465 (2019).
- [41] A. Silva, F. Monticone, G. Castaldi, V. Galdi, A. Alù, and N. Engheta, *Science* **343**, 160 (2014).
- [42] X. Xu, M. Tan, B. Corcoran, J. Wu, A. Boes, T. G. Nguyen, S. T. Chu, B. E. Little, D. G. Hicks, R. Morandotti, et al., *Nature* **589**, 44 (2021).
- [43] A. Babaee, A. Momeni, A. Abdolali, and R. Fleury, *Physical Review Applied* **15**, 044015 (2021).

[44] T. Wang, S.-Y. Ma, L. G. Wright, T. Onodera, B. C. Richard, and P. L. McMahon, *Nature Communications* **13**, 123 (2022).

[45] H. Rajabalipanah, A. Momeni, M. Rahmanzadeh, A. Abdolali, and R. Fleury, *Nanophotonics* **11**, 1561 (2022).

[46] P. del Hougne and G. Lerosey, *Physical Review X* **8**, 041037 (2018).

[47] A. Momeni, H. Rajabalipanah, M. Rahmanzadeh, A. Abdolali, K. Achouri, V. S. Asadchy, and R. Fleury, *IEEE Transactions on Antennas and Propagation* **69**, 7709 (2021).

[48] H. Zhou, J. Dong, J. Cheng, W. Dong, C. Huang, Y. Shen, Q. Zhang, M. Gu, C. Qian, H. Chen, et al., *Light: Science & Applications* **11**, 30 (2022).

[49] A. Momeni, M. Safari, A. Abdolali, N. P. Kherani, and R. Fleury, *Physical Review Applied* **15**, 034010 (2021).

[50] J. Sol, D. R. Smith, and P. del Hougne, *Nature Communications* **13**, 1 (2022).

[51] J. Sol, A. Alhulaymi, A. D. Stone, and P. del Hougne, *Science Advances* **9**, eadfo323 (2023).

[52] A. Rabault, L. L. Magoarou, J. Sol, G. C. Alexandropoulos, N. Shlezinger, H. V. Poor, and P. del Hougne, *arXiv:2302.04993* (2023).

[53] Y. Eliezer, U. Ruhrmair, N. Wisiol, S. Bittner, and H. Cao, *arXiv:2208.08906* (2022).

[54] U. Teğin, M. Yıldırım, İ. Oğuz, C. Moser, and D. Psaltis, *Nature Computational Science* **1**, 542 (2021).

[55] I. Oguz, J.-L. Hsieh, N. U. Dinc, U. Teğin, M. Yıldırım, C. Gigli, C. Moser, and D. Psaltis, *arXiv preprint arXiv:2208.04951* (2022).

[56] B. Rahmani, D. Loterie, E. Kakkava, N. Borhani, U. Teğin, D. Psaltis, and C. Moser, *Nature Machine Intelligence* **2**, 403 (2020).

[57] D. Loterie, S. Farahi, I. Papadopoulos, A. Goy, D. Psaltis, and C. Moser, *Optics express* **23**, 23845 (2015).